inorganics

MDPI

Article

Synthesis and Structure of ZnO-Decorated Graphitic Carbon Nitride (g-C_3N_4) with Improved Photocatalytic Activity under Visible Light

Maria I. Chebanenko [1,*], Sofia M. Tikhanova [1], Vladimir N. Nevedomskiy [2] and Vadim I. Popkov [1]

[1] Hydrogen Energy Laboratory, Ioffe Institute, 194021 Saint Petersburg, Russia
[2] Center of Nanoheterostructure Physics, Ioffe Institute, 194021 Saint Petersburg, Russia
* Correspondence: m_chebanenko@list.ru; Tel.: +7-(931)-213-25-76

Abstract: The volume of dye production in the chemical industry is growing rapidly every year. Given the global importance of clean water resources, new wastewater treatment solutions are required. Utilizing photocatalysis by harvesting solar energy represents a facile and promising solution for removing dangerous pollutants. This study reports the possibility of increasing the photocatalytic activity of g-C_3N_4 by creating nanocomposites with ZnO. Exfoliated g-C_3N_4/ZnO nanocomposites were synthesized by heat treatment of urea and subsequent ultrasonic exfoliation of the colloidal solution by introducing zinc acetate. The uniformity of the distribution of ZnO nanoparticles is confirmed by the method of elemental mapping. The obtained X-ray diffractograms of the obtained nanocomposites show typical X-ray reflections for g-C_3N_4 and ZnO. It was found that the introduction of oxide into g-C_3N_4 leads to an increase in the specific surface area values due to the developed ZnO surface. The maximum value of the specific surface area was obtained for a sample containing 7.5% ZnO and was 75.2 m^2/g. The g-C_3N_4/7.5% ZnO sample also demonstrated increased photocatalytic activity during the decomposition of methylene blue under the influence of visible light, which led to a twofold increase in the reaction rate compared to initial g-C_3N_4.

Keywords: graphitic carbon nitride; photocatalysts; g-C_3N_4/ZnO; visible light; photocatalytic degradation

check for updates

Citation: Chebanenko, M.I.; Tikhanova, S.M.; Nevedomskiy, V.N.; Popkov, V.I. Synthesis and Structure of ZnO-Decorated Graphitic Carbon Nitride (g-C_3N_4) with Improved Photocatalytic Activity under Visible Light. *Inorganics* **2022**, *10*, 249. https://doi.org/10.3390/inorganics10120249

Academic Editor: Roberto Nisticò

Received: 10 November 2022
Accepted: 6 December 2022
Published: 8 December 2022

1. Introduction

In the modern world, the rapid development of technology inevitably leads to an increase in the production of an ever-growing number of new chemical compounds. Such compounds are widely used in various industries [1–3]. Organic compounds, which are the basis of industrial dyes, are especially dangerous because their decomposition products can have a detrimental effect on living organisms when released into the environment [4,5]. Spreading through water, they can affect people and wildlife at a considerable distance from their original sources. Organic compounds also decompose at a slow rate and therefore accumulate and spread along the food chain. Consequently, when released into reservoirs with industrial wastewater, they disrupt the overall ecological balance of aquatic ecosystems [6,7]. In this regard, interest in the problem of industrial wastewater treatment has been growing recently.

Currently, physico-chemical, biological, and various other methods are used to solve this problem, which require expensive tools and can also lead to secondary contamination [8–12]. The photocatalytic decomposition process is a safe and effective method that can be used to remove organic pollutants from aquatic environments. Using this method, the photocatalyst converts toxic organic dyes into non-toxic intermediates under the influence of ultraviolet or visible light [13–16]. The development of such catalytic materials is an important task.

In past decade, nanoscale materials gained considerable importance due to their unique properties caused by scale factor absent in their bulk form. The reason for their

use in a large number of applications is due to their enhanced catalytic, optical, and electronic properties at the nano level. Nanoscale transition metal oxides are considered the most promising catalysts for wastewater treatment in a simple, reliable, fast, and environmentally friendly way considering their high photocatalytic activity, excellent solubility, and stability [17–22]. Among them, zinc oxide (ZnO) stands out especially. ZnO is a nontoxic, low-cost, and broadly available semiconductor that is widely used in photocatalytic degradation of organic dyes and photocatalytic decomposition of hydrogen generated from water. The nanostructured ZnO as compared to other nanostructures had gained importance because of ease in its fabrication and a number of applications. In order to use it as an efficient photocatalyst for the decomposition of organic pollutants, it is important to extend the work spectrum of ZnO from UV to the visible light region, increase a low specific surface area, and hinder the recombination of the photogenerated electron-hole pairs to improve the photocatalytic efficiency of ZnO [23]. To eliminate this disadvantage, it is proposed that new promising carbon-based materials be used as carriers [24,25]. One such material is graphite-like carbon nitride (g-C_3N_4). Due to its high stability and ability to absorb radiation in the visible region of the spectrum (band gap 2.4–2.9 eV), this compound has been widely used in the field of heterogeneous catalysis [26–28]. The use of g-C_3N_4 as a photocatalyst in the visible region of the spectrum was first reported in [29]. Unlike TiO_2, g-C_3N_4 does not contain noble or rare earth metal atoms in its composition, and it exhibits high photocatalytic activity in processes induced by the action of visible radiation [30–33]. Materials based on g-C_3N_4 can be considered as a promising basis for new functional materials for photocatalysis.

Therefore, the main objective of this paper is the synthesis of a nanocomposite based on g-C_3N_4 and ZnO with improved photocatalytic properties. The novelty of the presented research lies in the use of an improved synthetic route. A special feature is the ultrasonic dispersion of g-C_3N_4, preceding the introduction of zinc acetate. The positive effect of this exfoliation method was previously reported in [34–36]. As a result, the synthesized g-C_3N_4/ZnO powders demonstrate a small band gap and a large surface area, as well as an improved ability to absorb visible radiation and an increase in the photodegradation rate of organic pollutants in composite nanoplanes.

2. Results and Discussion

Figure 1 shows the results of an X-ray diffraction of the obtained powders. The diffractogram of pure g-C_3N_4 contains X-ray peaks typical of graphite-like carbon nitride [37,38]. The most intense peak is located in the region of 27.4° and is associated with the characteristic interlayer stacking of conjugated aromatic rings. A less intense peak at 12.8° corresponds with the layered structure of the packing of tri-s-triazine units, which corresponds with the plane (100) in the JCPDS 87-1526 card. ZnO peaks are traced on diffractograms of the obtained nanocomposites. The intensity of the peaks increases with an increase in the mass fraction of the oxide in the samples. All detectable X-ray reflections of ZnO can be indexed by the wurtzite structure (JCPDS No. 36-1451). It is noted that the presence of oxide does not affect the position of the diffraction peaks of g-C_3N_4, and a slight change in the relative intensity of the peak reflects only the ratio of the components.

The microstructure of the obtained samples is studied using scanning electron microscopy. The pure g-C_3N_4 sample consists of randomly stacked layers consisting of inhomogeneously distributed and agglomerated structures (Figure 2a,b). In the sample containing 7.5% ZnO (Figure 2c,d), the nanolayers are randomly filled with oxide nanoparticles (NPs). Nanocomposite powders look less agglomerated and have a friable structure.

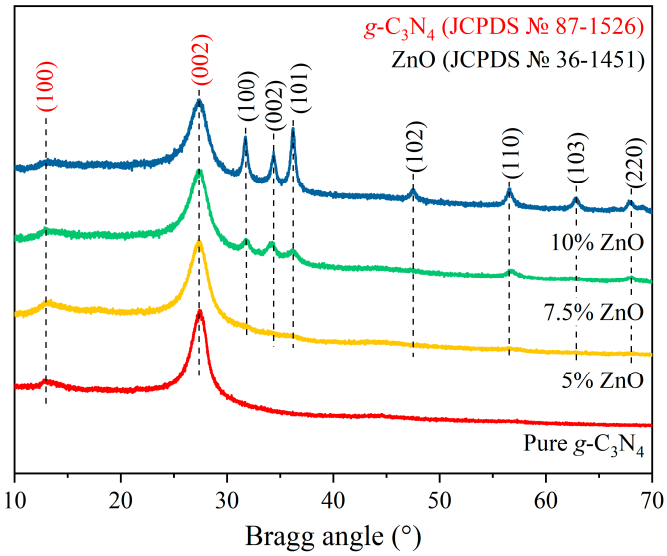

Figure 1. PXRD patterns of the initial g-C_3N_4, g-C_3N_4/ZnO (5% ZnO, 7.5% ZnO, and 10% ZnO) nanocomposites.

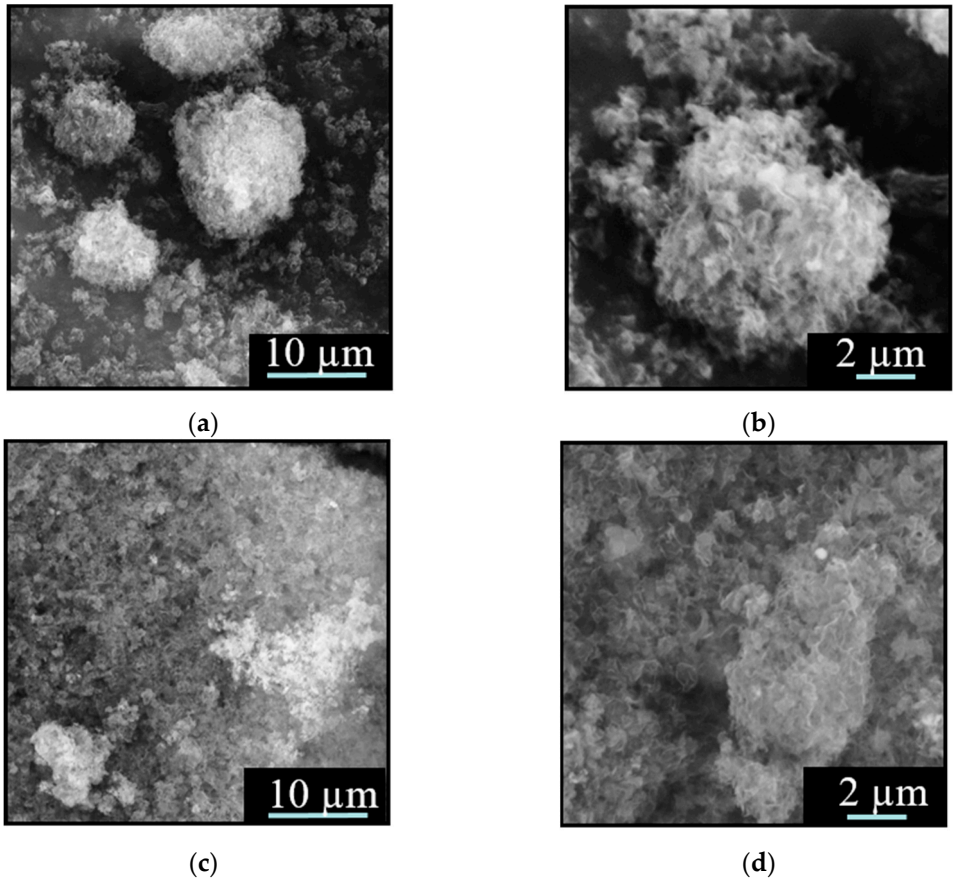

Figure 2. SEM images of (**a**,**b**) pure g-C_3N_4 and (**c**,**d**) g-C_3N_4/7.5% ZnO.

X-ray spectroscopy (EDX) elemental mapping results are shown in Figure 3. The elemental mapping results indicate the existence of C, N, Zn, and O elements suggesting that ZnO NPs disperse on the g-C_3N_4 sheets. A uniform distribution of C, N, Zn, and O atoms could be observed throughout each entire nanoplate.

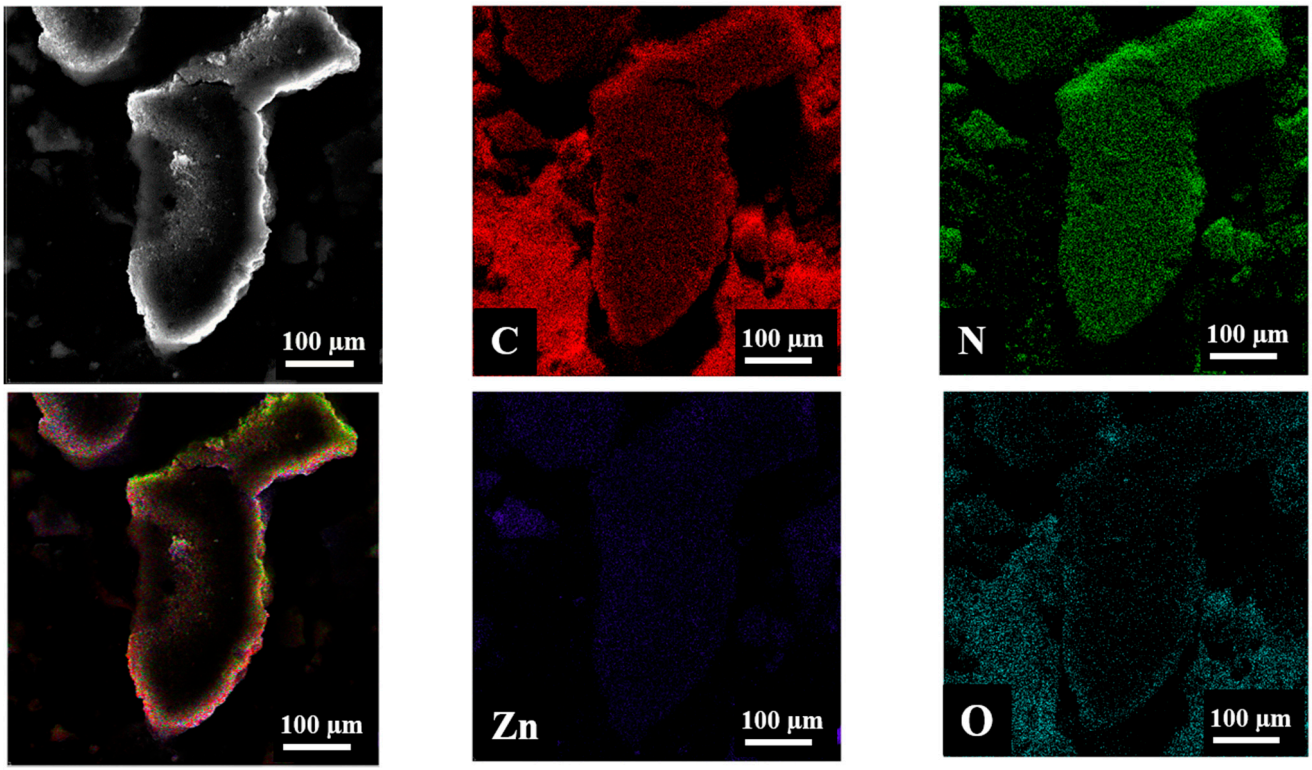

Figure 3. EDX mapping of g-C_3N_4/7.5% ZnO nanocomposite.

Using TEM and SAED, the surface morphologies and structural characteristics of g-C_3N_4/7.5% ZnO nanocomposite were analyzed. Previously, a TEM image of pure g-C_3N_4 was shown in [35], where the morphology consists of agglomerated planes. According to the comparison of the TEM data measured in bright field and dark field modes (Figure 4a and 4b, respectively), ZnO nanocrystals are uniformly located throughout the sample volume, which is consistent with the results of elemental mapping. ZnO can be clearly observed as a cluster of irregularly shaped NPs, and g-C_3N_4 looks like dimmer sections of two-dimensional layered structures, which indicates the presence of a number of stacked layers. The g-C_3N_4 layers are compacted with ZnO NPs and have close contact between g-C_3N_4 and ZnO, which is required to form a heterojunction and achieve better charge separation. The diffraction ring positions in SAED patterns of the nanocomposite (Figure 4c) match the known interplanar distances in ZnO and g-C_3N_4 and confirm that individual nanocrystals observed in dark-field mode correspond to ZnO. Figure 4d shows an HRTEM image in which the ZnO lattice planes were detected at 7.5 wt% g-C_3N_4/ZnO composite [39]. The results of X-ray diffraction and TEM confirm that ZnO nanocrystals having (002) crystallographic phases on their surfaces are in direct contact with g-C_3N_4.

N_2 adsorption-desorption isotherms of pure g-C_3N_4 and g-C_3N_4/7.5% ZnO were measured to gain information about the specific surface area (Figure 5a). According to the International Union of Pure and Applied Chemistry (IUPAC) classification, obtained isotherms were determined as type III with mesoporous characteristics, which indicates the mesoporous structure of the samples. The pore size distribution of the samples shows that most of the pores fall into the size range from 2 to 50 nm. The specific surface area values are shown in Figure 5b. The surface area for the resulting samples was calculated using the Brunauer–Emmet–Teller (BET) equation in the range of relative pressure (P/P_0) 0.05–0.3. The specific surface area of the samples determined by the BET method is 34.4, 54.5, 75.2, and 68.5 m^2/g for g-C_3N_4, g-C_3N_4/5% ZnO, g-C_3N_4/7.5% ZnO, and g-C_3N_4/10% ZnO, respectively. The optimal amount of oxide in the nanocomposite is 7.5 wt% ZnO, while further increase leads to a decrease in the values of the specific surface area. The surface of

the composite samples will absorb more visible light, thereby increasing the photocatalytic efficiency by providing more active centers.

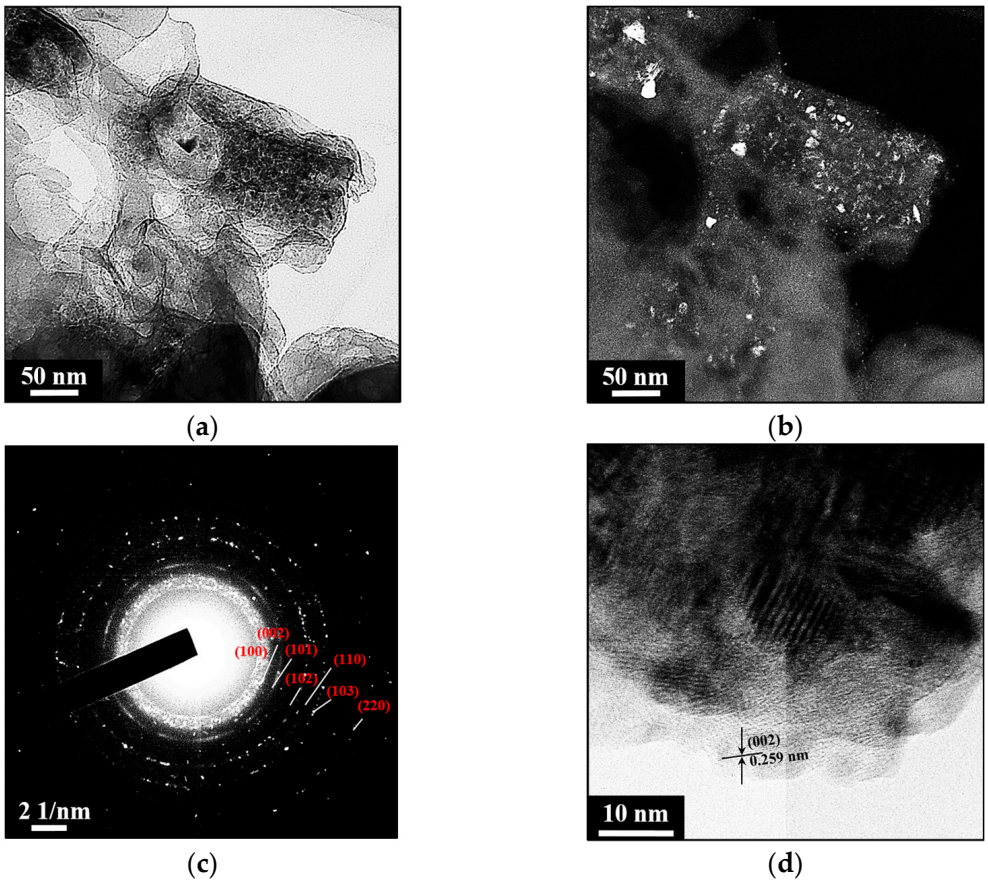

Figure 4. (**a**) The bright-field and (**b**) dark-field transmission electron microscopy (TEM) image of g-C_3N_4/7.5% ZnO NPs, (**c**) selected area electron diffraction (SAED) pattern, and (**d**) high resolution-TEM (HR-TEM) image.

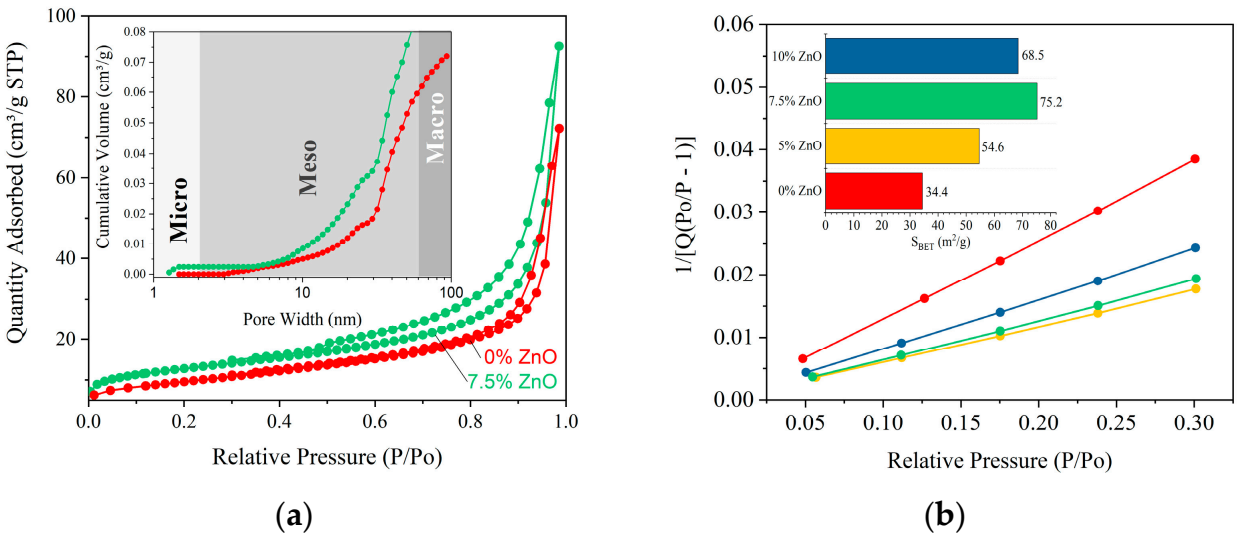

Figure 5. (**a**) N_2 adsorption-desorption isotherms of initial g-C_3N_4 and g-C_3N_4/7.5% ZnO samples; (**b**) BET surface area plot of initial g-C_3N_4 and g-C_3N_4/ZnO nanocomposites.

The UV–vis DRS of all samples is demonstrated in Figure 6a. It can be seen that the absorption of light by g-C_3N_4 is lower than that of other samples. When g-C_3N_4 is recombined with ZnO, the light absorption band edge undergoes a slight red shift. Such a modest change in the distance between the bands may indicate a tight contact at the interface with g-C_3N_4 and ZnO and confirms the synthesis of the nanocomposite. To further study the photocatalytic effect of the composites, a Tauc plot was derived from the UV-vis spectrum.

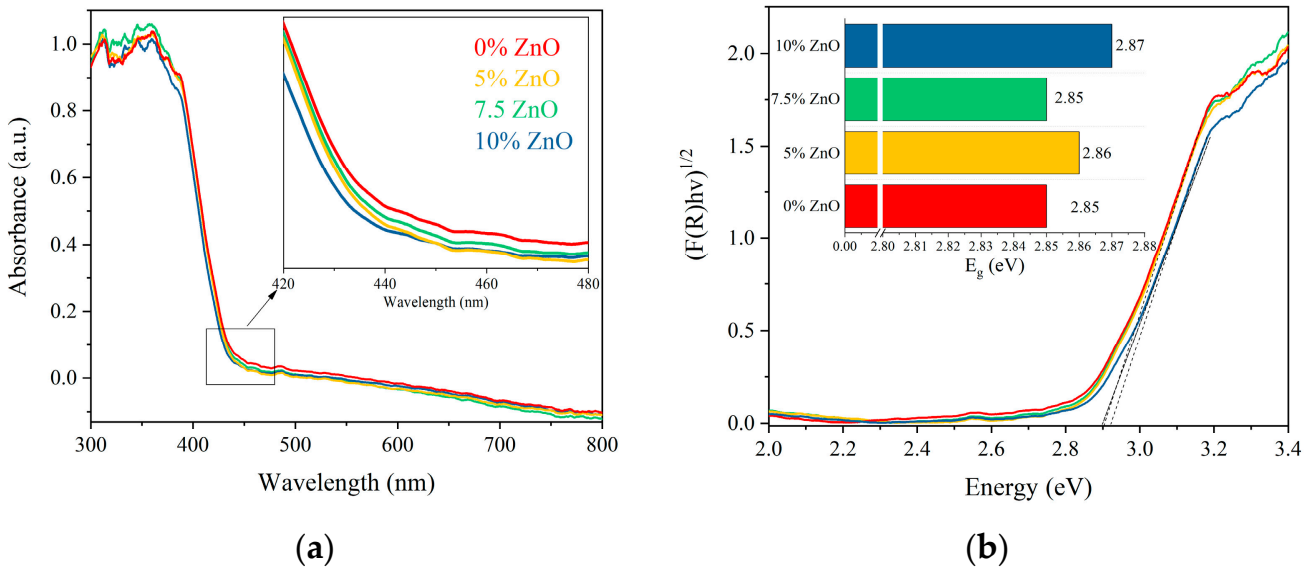

(**a**) (**b**)

Figure 6. (**a**) UV-vis DRS and (**b**) Tauc Plots of the initial g-C_3N_4 and g-C_3N_4/ZnO (5% ZnO, 7.5% ZnO and 10% ZnO) nanocomposites.

The addition of ZnO results in a moderate modification of Tauc plots, as illustrated in Figure 6b. As a result of the shift in absorbance edges for the nanocomposite structure, the band gaps for g-C_3N_4 and g-C_3N_4/ZnO (5% ZnO, 7.5% ZnO, and 10% ZnO) are 2.85, 2.86, 2.85, and 2.87 eV, respectively. It is reported above that the nanocomposite has a larger contact interface area (Figure 5), which allows faster charging carrier transit and, therefore, suppresses charge recombination, leading to increased photocatalytic degradation efficiency.

All samples were examined for their photocatalytic potential towards photodegradation of MB dye solution. Figure 7a shows the absorption spectra of the dye solution with samples under visible light irradiation at 10-min intervals. It can be seen from Figure 7b that the degradation of methylene blue by g-C_3N_4 in the dark is negligible. After g-C_3N_4 is compounded with oxide, its photocatalytic efficiency is further improved. The degradation of MB is analyzed by pseudo-first order kinetics (Figure 7c). The degradation of MB practically did not proceed in the blank experiment, which illustrates MB can not be degraded under visible irradiation. The experiment reveals that MB could be degraded at a rate constant 2.2×10^{-3} min^{-1}, 3.2×10^{-3} min^{-1}, 4.6×10^{-3} min^{-1}, and 3.2×10^{-3} min^{-1} using g-C_3N_4, g-C_3N_4/5% ZnO, g-C_3N_4/7.5% ZnO, and g-C_3N_4/10% ZnO, respectively. In the present study, a 7.5% ZnO sample shows better photodegradation performance as compared to others. This effect is explained by the optimal ratio of components in the nanocomposite, which positively affects the size of the specific surface area and the availability of active centers. The rate constant of g-C_3N_4/7.5% ZnO is about two times higher than that of pure g-C_3N_4. The results reveal that a certain proportion of ZnO has the best photocatalytic activity.

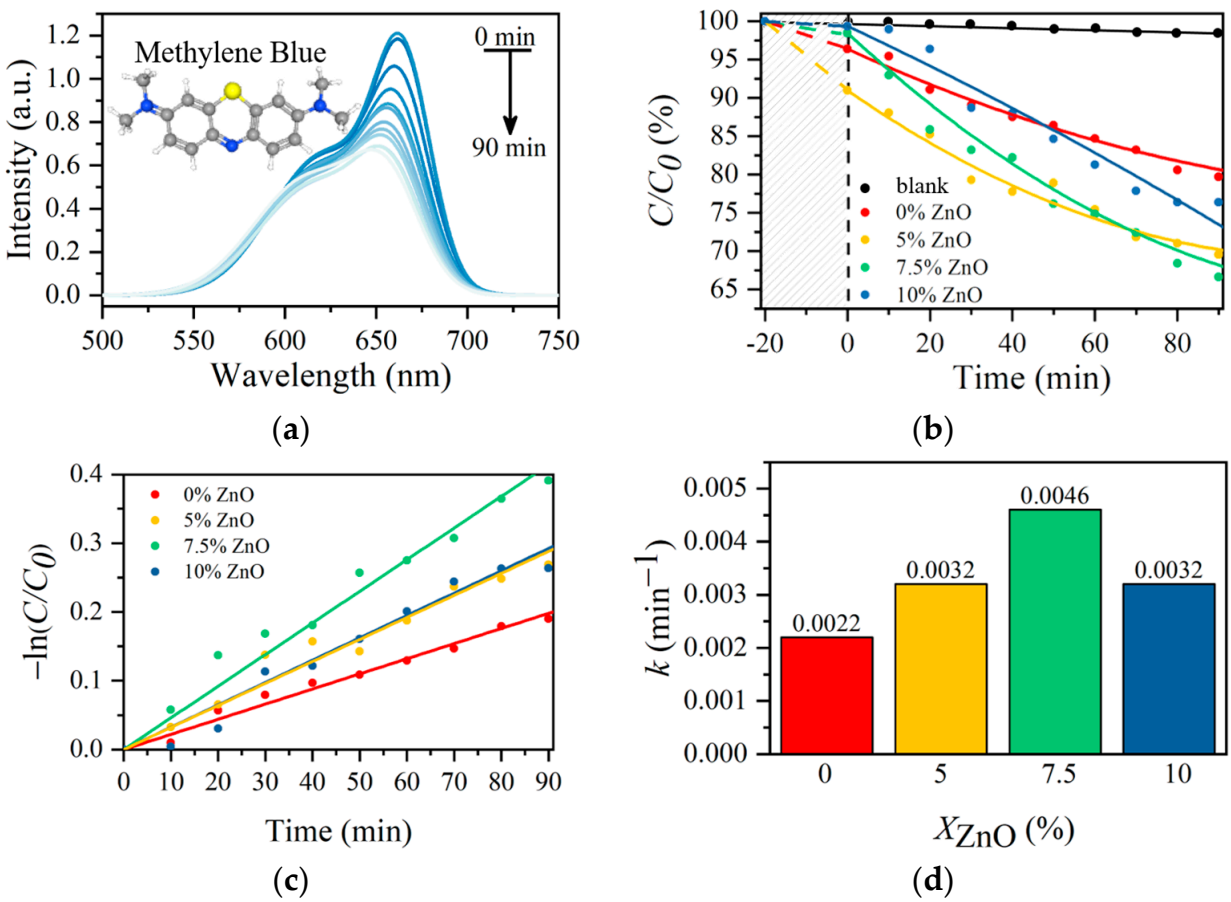

Figure 7. (**a**) Photocatalytic degradation of MB over g-C_3N_4/7.5% ZnO catalyst under visible light; (**b**) Kinetic curves, (**c**) Logarithmic kinetic curves of the pseudo-first-order process; (**d**) Photodecomposition rate constant versus ZnO content.

Photoluminescence (PL) spectra were obtained to study the processes of charge carrier transfer. Evaluation of the efficiency of carrier separation will additionally confirm the improvement of the photocatalytic characteristics of photocatalysts. Photoluminescence emission spectra of the prepared samples were recorded at an excitation wavelength of 365 nm and are shown in Figure 8a. All samples demonstrated a peak of PL radiation in a similar region between 400 and 500 nm. A decrease in the photoluminescence intensity for g-C_3N_4/ZnO nanocomposites indicated that the high-efficiency electron transferred from the conduction band of g-C_3N_4 to the conduction band of ZnO hindered the reorganization of photoinduced charge carriers. This indicates that the recombination rate of electrons and holes under visible light irradiation is lower in this case. This leads to higher charge separation, which can provide more electrons for photocatalytic activity.

The stability of the g-C_3N_4/7.5% ZnO was examined by recycling the photocatalyst for the photocatalytic degradation of MB dye. After each cycle, the catalyst particles were collected by centrifugation, washed with distilled water, and dried at 60 °C. Then the particles were reused, and the dye solution was replaced with a fresh one. As shown in Figure 8b, no major reduction was observed in the efficiency after four consecutive cycles; as a result, the g-C_3N_4/7.5% ZnO photocatalysts were photostable.

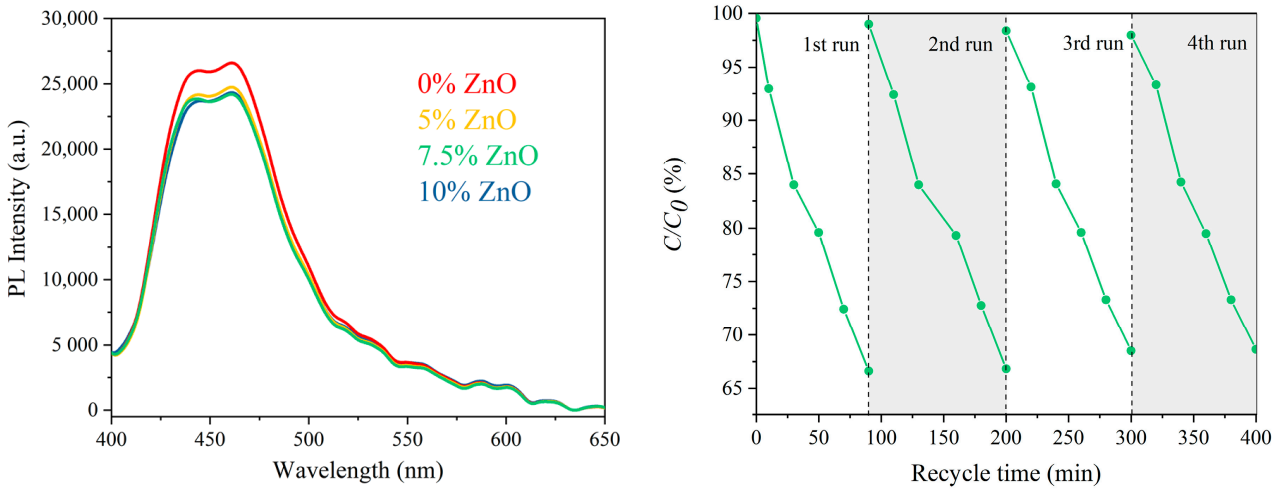

(**a**) (**b**)

Figure 8. (**a**) PL spectra of initial g-C_3N_4 and g-C_3N_4/ZnO (5% ZnO, 7.5% ZnO and 10% ZnO) nanocomposites; (**b**) Recycling photocatalytic test of g-C_3N_4/7.5% ZnO.

Figure 9 shows the mechanism of photocatalytic degradation of MB by g-C_3N_4/ZnO nanocomposites. ZnO has a band gap of about 3.37 eV [40,41] and cannot be excited by visible light. The spectrum of the g-C_3N_4/ZnO composite can be broadened to the visible region in contrast to pure ZnO. g-C_3N_4 is activated by sunlight, causing the electrons to shift from the valence band (VB) of each sample to the conduction band (CB) and create h^+ on the VB of g-C_3N_4. These excited electrons are then transferred to the CB of ZnO, which further promoted it to the surface, leading to the generation of O_2^- radicals. The holes in the VB of ZnO are transferred to the VB of g-C_3N_4, which ensure effective charge separation in the system. These VB holes in g-C_3N_4 are further transferred to the surface to react with surrounding molecules and generate ·OH radicals [42,43]. In this way, these generated radicals are actively involved in the degradation of dye molecules.

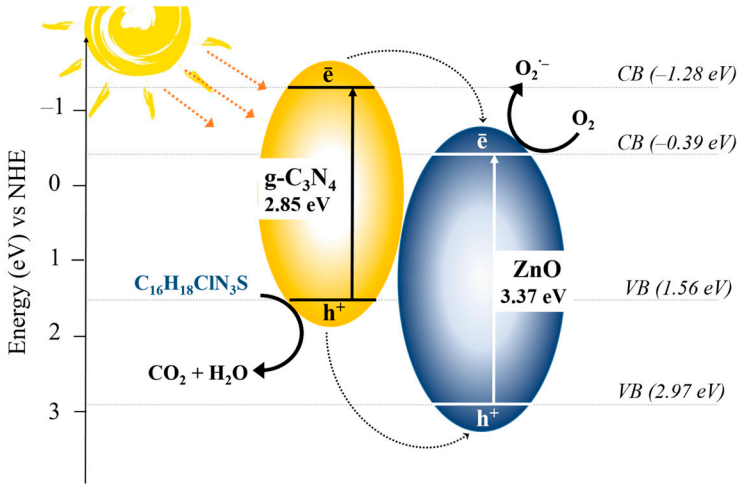

Figure 9. Schematic mechanism of photocatalytic degradation of MB of g-C_3N_4/ZnO under visible light.

3. Materials and Methods

3.1. Materials

Zinc acetate dihydrate ($Zn(CH_3COO)_2 \cdot H_2O$, NevaReaktiv, Saint-Petersburg, Russia) was used as a precursor for ZnO. Graphitic carbon nitride was prepared from urea (CH_4N_2O, NevaReaktiv, Saint-Petersburg, Russia). Methylene blue ($C_{16}H_{18}ClN_3S$, LenReak-

tiv, Saint-Petersburg, Russia) was used as model dye. All the reagents used in this research work are analytical grade.

3.2. Synthesis of Initial g-C_3N_4 Nanopowder

The initial *g*-C_3N_4 nanopowder was synthesized via heat treatment of 10 g urea for 1 h in a muffle furnace in air atmosphere. A dry powder of urea was placed in a quartz tube heated to 550 °C at a fixed heating rate of 5°/min. As a result of the heat treatment, a powder of pale-yellow color was obtained.

3.3. Synthesis of Exfoliated g-C_3N_4/ZnO Nanocomposites

To obtain nanocomposites based on g-C_3N_4 and ZnO, the following procedure was performed. The initial sample was treated by ultrasonic dispersion in distilled water for 2 h until a milk-colored homogenized suspension was obtained. The resulting suspension was divided into four equal portions, to each of which the necessary amount of $Zn(CH_3COO)_2 \cdot 2H_2O$ was added and thoroughly mixed using a magnetic stirrer. Further, the obtained suspensions were dried at 100 °C until the water was completely removed, thoroughly ground, and treated thermally at 400 °C. As a result, a series of four samples was obtained: g-C_3N_4, g-C_3N_4-ZnO 5%, g-C_3N_4-ZnO 7.5%, and g-C_3N_4-ZnO 10%.

3.4. Physico-Chemical Characterization

The crystal phases of the catalysts were analyzed by powder X-ray diffraction patterns (XRD) using a Rigaku SmartLab 3 diffractometer (Rigaku Corporation, Tokyo, Japan) (CuKα radiation, λ = 0.154051 nm). The measurement was conducted by varying the Bragg angle in the range of 10–80°.

The elemental composition and morphology of nanopowders was studied with scanning electron microscopy (SEM) using a Tescan Vega 3 SBH (Tescan, Czech Republic) scanning electron microscope with an Oxford INCA x-act X-ray microanalysis device (Oxford Instruments, UK). An Oxford Instruments INCA system was used for chemical analysis, including elemental mapping utilizing a 10 nm probe size.

The microstructure and morphology evaluation were investigated by Transmission Electron Microscopy (TEM) using a JEOL JEM2100F microscope (JEOL Ltd., Tokyo, Japan) in the image and selected area electron diffraction (SAED) mode.

Measurement of N_2 adsorption-desorption was carried out for specific surface area and pore structure analysis (ASAP 2020 Surface Area and Porosity Analyzer Micromeritics, Micromeritics Instrument Corporation, Norcross, GA, USA) in standard mode at 78 K, the temperature of liquid nitrogen.

Diffuse reflectance spectra of samples were obtained using an Avaspec-ULS2048CL-EVO spectrometer (Avantes, Apeldoorn, The Netherlands) equipped with an AvaSphere-30-REFL refractometric integration sphere in the 350–700 nm region.

3.5. Photocatalytic Measurements

Photocatalytic activity of synthesized nanocomposites was studied by measuring the change in the absorption spectra of methylene blue ($C_{16}H_{18}ClN_3S$, MB) under visible light irradiation. For the test, 0.01 g of the nanocomposite was placed in a solution of MB (10 mg/l). The prepared suspensions were continuously mixed for 20 min in the dark to establish sorption equilibrium. Then the samples were constantly mixed at a temperature of 25 °C throughout the analysis in a closed box under the illumination of an Xe lamp (power consumption 70 W, λ_{max} = 410 nm). Aliquots of samples were taken at intervals of 10 min during the 90 min of the experiment. All samples were centrifuged to remove solid particles, and the supernatant was analyzed using an Avaspec-ULS2048CL-EVO spectrometer equipped with an Avalight-XE Pulsed Xenon Lamp (Avantes, Apeldoorn, The Netherlands).

4. Conclusions

In this work, nanocrystalline g-C_3N_4/ZnO powders were obtained by heat treatment of a mixture of g-C_3N_4 and zinc acetate. The resulting series of samples (pure g-C_3N_4, g-C_3N_4/5% ZnO, g-C_3N_4/7.5% ZnO, and g-C_3N_4/10% ZnO) was studied using a complex of physico-chemical analysis methods. The ZnO NPs were evenly distributed on the surface and represented a crystalline modification with a wurtzite structure. The specific surface area of the powder reached its maximum value at 7.5% of ZnO content. A further increase in the amount of ZnO in the composition led to a decrease in the values of the specific surface area. This structure of the Z-scheme led to an increase in the photocatalytic activity of the studied nanocomposite. Compared with pure material, g-C_3N_4/7.5% ZnO showed a much greater photocatalytic activity. Thus, g-C_3N_4/ZnO is practically suitable for the photocatalytic decomposition of organic materials under visible light.

Author Contributions: Conceptualization, M.I.C. and V.I.P.; methodology, M.I.C.; software, M.I.C. and S.M.T.; validation, M.I.C.; formal analysis, M.I.C. and S.M.T.; investigation, M.I.C. and S.M.T.; resources, V.I.P. and V.N.N.; data curation, M.I.C.; writing—original draft preparation, M.I.C. and S.M.T.; writing—review and editing, M.I.C. and V.I.P.; visualization, V.N.N.; supervision, V.I.P.; project administration, V.I.P. All authors have read and agreed to the published version of the manuscript.

Funding: This research received no external funding.

Acknowledgments: The author would like to thank M.I. Tenevich for help with scanning electron microscopy studies.

Conflicts of Interest: The authors declare no conflict of interest.

References

1. Shannon, M.A.; Bohn, P.W.; Elimelech, M.; Georgiadis, J.G.; Marin, B.J.; Mayes, A.M. Science and technology for water purification in the coming decades. *Nature* **2008**, *452*, 301–310. [CrossRef] [PubMed]
2. Nasrollahzadeh, M.; Sajjadi, M.; Iravani, S.; Varma, R.S. Green-synthesized nanocatalysts and nanomaterials for water treatment: Current challenges and future perspectives. *J. Hazard. Mater.* **2020**, *401*, 123401. [CrossRef] [PubMed]
3. Nayak, S.; Mohapatra, L.; Parida, K. Visible light-driven novel g-C_3N_4/NiFe-LDH composite photocatalyst with enhanced photocatalytic activity towards water oxidation and reduction reaction. *J. Mater. Chem. A* **2015**, *3*, 18622–18635. [CrossRef]
4. Mahmood, A.; Muhmood, T.; Ahmad, F. Carbon nanotubes heterojunction with graphene like carbon nitride for the enhancement of electrochemical and photocatalytic activity. *Mater. Chem. Phys.* **2022**, *278*, 125640. [CrossRef]
5. Muhmood, T.; Xia, M.; Lei, W.; Wang, F. Under vacuum synthesis of type-I heterojunction between red phosphorus and graphene like carbon nitride with enhanced catalytic, electrochemical and charge separation ability for photodegradation of an acute toxicity category-III compound. *Appl. Catal. B Environ.* **2018**, *238*, 568–575. [CrossRef]
6. Ren, Q.; Nie, M.; Yang, L.; Wei, F.; Ding, B.; Chen, H.; Liu, Z.; Liang, Z. Synthesis of MOFs for RhB Adsorption from Wastewater. *Inorganics* **2022**, *10*, 27. [CrossRef]
7. Lee, Y.-G.; Chon, K. Green Technologies for Sustainable Water and Wastewater Treatment: Removal of Organic and Inorganic Contaminants. *Separations* **2022**, *9*, 335. [CrossRef]
8. Klaczyński, E.; Ratajczak, P. Oczyszczalnie ścieków—Układy technologiczne (Waste water treatment plants—Process systems). *Wodociągi Kanaliz.* **2013**, *4*, 36–39.
9. Narayanan, C.M.; Narayan, V. Biological wastewater treatment and bioreactor design: A review. *Sustain. Environ. Res.* **2019**, *29*, 33. [CrossRef]
10. Vukšić, M.; Kocijan, M.; Ćurković, L.; Radošević, T.; Vengust, D.; Podlogar, M. Photocatalytic Properties of Immobilised Graphitic Carbon Nitride on the Alumina Substrate. *Appl. Sci.* **2022**, *12*, 9704. [CrossRef]
11. Kocijan, M.; Ćurković, L.; Radošević, T.; Podlogar, M. Enhanced Photocatalytic Activity of Hybrid rGO@TiO_2/CN Nanocomposite for Organic Pollutant Degradation under Solar Light Irradiation. *Catalysts.* **2021**, *11*, 1023. [CrossRef]
12. Kocijan, M.; Ćurković, M.; Gonçalves, G.; Podlogar, M. The Potential of rGO@TiO_2 Photocatalyst for the Degradation of Organic Pollutants in Water. *Sustainability* **2022**, *14*, 12703. [CrossRef]
13. Srivastava, R.R.; Vishwakarma, P.K.; Yadav, U.; Rai, S.; Umrao, S.; Giri, R.; Saxena, P.S.; Srivastava, A. 2D SnS_2 Nanostructure-Derived Photocatalytic Degradation of Organic Pollutants Under Visible Light. *Front. Nanotechnol.* **2021**, *3*, 711368. [CrossRef]
14. Lebedev, L.A.; Chebanenko, M.I.; Dzhevaga, E.V.; Martinson, K.D.; Popkov, V.I. Solvothermal modification of graphitic C_3N_4 with Ni and Co phthalocyanines. *Mendeleev Commun.* **2022**, *32*, 317–319. [CrossRef]
15. Kocijan, M.; Ćurković, L.; Ljubas, D.; Mužina, K.; Bačić, I.; Radošević, T.; Podlogar, M.; Bdikin, I.; Otero-Irurueta, G.; Hortigüela, M.J.; et al. Graphene-Based TiO_2 Nanocomposite for Photocatalytic Degradation of Dyes in Aqueous Solution under Solar-Like Radiation. *Appl. Sci.* **2021**, *11*, 3966. [CrossRef]

16. Kocijan, M.; Ćurković, L.; Bdikin, I.; Otero-Irurueta, G.; Hortigüela, M.J.; Gonçalves, G.; Radošević, T.; Vengust, T.; Podlogar, M. Immobilised rGO/TiO_2 Nanocomposite for Multi-Cycle Removal of Methylene Blue Dye from an Aqueous Medium. *Appl. Sci.* **2022**, *12*, 385. [CrossRef]
17. Nazim, M.; Parwaz Khan, A.A.; Asiri, A.M.; Kim, J.H. Exploring Rapid Photocatalytic Degradation of Organic Pollutants with Porous CuO Nanosheets: Synthesis, Dye Removal, and Kinetic Studies at Room Temperature. *ACS Omega* **2021**, *6*, 2601–2612. [CrossRef]
18. Lasio, B.; Malfatti, L.; Innocenzi, P. Photodegradation of Rhodamine 6G dimers in silica sol-gel films. *J. Photochem. Photobiol.* **2013**, *271*, 93–98. [CrossRef]
19. Buthiyappan, A.; Abdul Aziz, A.R.; Wan Daud, W.M.A.; Daud, W. Recent advances and prospects of catalytic advanced oxidation process in treating textile effluents. *Rev. Chem. Eng.* **2016**, *32*, 1–47. [CrossRef]
20. Shi, S.; Xu, J.; Li, L. Preparation and Photocatalytic Activity of ZnO Nanorods and ZnO/Cu_2O Nanocomposites. *Main Group Chem.* **2017**, *16*, 47–55. [CrossRef]
21. Chebanenko, M.I.; Martinson, K.D.; Matsukevich, I.V.; Popkov, V.I. The effect of MgO additive on the g-C_3N_4 performance in electrochemical reforming of water-ethanol solution. *Nanosyst. Phys. Chem. Math.* **2020**, *11*, 474–479. [CrossRef]
22. Pant, B.; Park, M.; Hee Lee, J.; Kim, H.-Y.; Park, S.-J. Novel magnetically separable silver-iron oxide nanoparticles decorated graphitic carbon nitride nano-sheets: A multifunctional photocatalyst via one-step hydrothermal process. *J. Colloid Interface Sci.* **2017**, *496*, 343–352. [CrossRef]
23. Pant, B.; Park, M.; Kim, H.-Y.; Park, S.-J. Ag-ZnO photocatalyst anchored on carbon nanofibers: Synthesis, characterization, and photocatalytic activities. *Synth. Met.* **2016**, *220*, 533–537. [CrossRef]
24. Elshafie, M.; Younis, S.A.; Serp, P.; Gad, E.A.M. Preparation characterization and non-isothermal decomposition kinetics of different carbon nitride sheets. *Egypt. J. Pet.* **2019**, *29*, 21–29. [CrossRef]
25. Huang, R.; Wu, J.; Zhang, M.; Liu, B.; Zheng, Z.; Luo, D. Strategies to enhance photocatalytic activity of graphite carbon nitride-based photocatalysts. *Mater. Des.* **2019**, *210*, 110040. [CrossRef]
26. Muhmood, T.; Asim Khan, M.; Xia, M.; Lei, W.; Wang, F.; Ouyang, Y. Enhanced photo-electrochemical, photo-degradation and charge separation ability of graphitic carbon nitride (g-C_3N_4) by self-type metal free heterojunction formation for antibiotic degradation. *J. Photochem. Photobiol. A Chem.* **2017**, *348*, 118–124. [CrossRef]
27. Zhao, L.; Zhang, L.; Lin, H.; Nong, Q.; Cui, M.; Wu, Y.; He, Y. Fabrication and characterization of hollow $CdMoO_4$ coupled g-C_3N_4 heterojunction with enhanced photocatalytic activity. *J. Hazard. Mater.* **2015**, *299*, 333–342. [CrossRef]
28. Sun, S.; Ding, H.; Mei, L.; Chena, Y.; Hao, Q.; Chen, W.; Xu, Z.; Chen, D. Construction of SiO_2-TiO_2/g-C_3N_4 composite photocatalyst for hydrogen production and pollutant degradation: Insight into the effect of SiO_2. *Chin. Chem. Lett.* **2020**, *31*, 2287–2294. [CrossRef]
29. Mo, Z.; She, X.; Li, Y.; Liu, L.; Huang, L.; Chen, Z.; Zhang, Q.; Xu, H.; Li, H. Synthesis of g-C_3N_4 at different temperatures for superior visible/UV photocatalytic performance and photoelectrochemical sensing of MB solution. *RSC Adv.* **2015**, *5*, 101552–101562. [CrossRef]
30. Maeda, K.; Wang, X.; Nishihara, Y.; Lu, D.; Antonietti, M.; Domen, K. Photocatalytic Activities of Graphitic Carbon Nitride Powder for Water Reduction and Oxidation under Visible Light. *J. Phys. Chem. C* **2009**, *113*, 4940–4947. [CrossRef]
31. Dong, F.; Wu, L.; Sun, Y.; Fu, M.; Wu, Z.; Lee, S.C. Efficient synthesis of polymeric g-C_3N_4 layered materials as novel efficient visible light driven photocatalysts. *J. Mater. Chem.* **2011**, *21*, 15171–15174. [CrossRef]
32. Kharlamov, A.; Bondarenko, M.; Kharlamova, G.; Gubareni, N. Features of the synthesis of carbon nitride oxide (g-C_3N_4)O at urea pyrolysis. *Diam. Relat. Mater.* **2016**, *66*, 16–22. [CrossRef]
33. Chidhambaram, N.; Ravichandran, K. Single step transformation of urea into metal-free g-C_3N_4 nanoflakes for visible light photocatalytic applications. *Mater. Lett.* **2017**, *207*, 44–48. [CrossRef]
34. Chebanenko, M.I.; Zakharova, N.V.; Lobinsky, A.A.; Popkov, V.I. Ultrasonic-Assisted Exfoliation of Graphitic Carbon Nitride and its Electrocatalytic Performance in Process of Ethanol Reforming. *Semiconductors* **2019**, *53*, 28–33. [CrossRef]
35. Chebanenko, M.I.; Lobinsky, A.A.; Nevedomskiy, V.N.; Popkov, V.I. NiO-decorated Graphitic Carbon Nitride toward Electrocatalytic Hydrogen Production from Ethanol. *Dalton Trans.* **2020**, *49*, 12088–12097. [CrossRef] [PubMed]
36. Chebanenko, M.I.; Lebedev, L.A.; Ugolkov, V.L.; Prasolov, N.D.; Nevedomskiy, V.N.; Popkov, V.I. Chemical and structural changes of g-C_3N_4 through oxidative physical vapor deposition. *Appl. Surf. Sci.* **2022**, *600*, 154079. [CrossRef]
37. Muhmood, T.; Xia, M.; Lei, W.; Wang, F.; Mahmood, A. Fe-ZrO_2 imbedded graphene like carbon nitride for acarbose (ACB) photo-degradation intermediate study. *Adv. Powder Technol.* **2018**, *29*, 3233–3240. [CrossRef]
38. Muhmood, T.; Xia, M.; Lei, W.; Wang, F.; Khan, M.A. Design of Graphene Nanoplatelet/Graphitic Carbon Nitride Heterojunctions by Vacuum Tube with Enhanced Photocatalytic and Electrochemical Response. *ur. J. Inorg. Chem.* **2018**, *2018*, 1726–1732. [CrossRef]
39. Xiuling Guo, X.; Duan, J.; Li, C.; Zhang, Z.; Wang, W. Highly efficient Z-scheme g-C_3N_4/ZnO photocatalysts constructed by co-melting-recrystallizing mixed precursors for wastewater treatment. *J. Mater. Sci.* **2020**, *55*, 2018–2031. [CrossRef]
40. Wang, M.; Jiang, L.; Kim, E.J.; Hahn, S.H. Electronic structure and optical properties of $Zn(OH)_2$: LDA+U calculations and intense yellow luminescence. *RSC Adv.* **2015**, *5*, 87496. [CrossRef]
41. Guan, R.; Li, J.; Zhang, J.; Zhao, Z.; Wang, D.; Zhai, H.; Sun, D. Photocatalytic Performance and Mechanistic Research of ZnO/g-C_3N_4 on Degradation of Methyl Orange. *ACS Omega* **2019**, *4*, 20742–20747. [CrossRef]

42. Gayathri, M.; Sakar, M.; Satheeshkumar, E.; Sundaravadivel, E. Insights into the mechanism of ZnO/g-C_3N_4 nanocomposites toward photocatalytic degradation of multiple organic dyes. *J. Mater. Sci. Mater. Electron.* **2022**, *33*, 9347–9357. [CrossRef]
43. Alharthi, F.A.; Alghamdi, A.A.; Alanazi, H.S.; Alsyahi, A.A.; Ahmad, N. Photocatalytic Degradation of the Light Sensitive Organic Dyes: Methylene Blue and Rose Bengal by Using Urea Derived g-C_3N_4/ZnO Nanocomposites. *Catalysts.* **2020**, *10*, 1457. [CrossRef]